discontinuity may be produced by the local gradients caused by thermal variations alone without a need for a first-order discontinuity. Although such a possibility has long been acknowledged by the seismological community (*10*), it is unlikely that thermal gradients of sufficient sharpness (*5*) can be produced. Dynamically consistent seismic velocity gradients constrained by mineral physics data (*11*) are not capable of producing a triplication consistent with observations. Similarly, no triplication is produced by the seismic velocity gradients obtained from tomography inversions (*18*).

24. This is not immediately obvious, considering some degree of smoothing that occurs in tomographic inversions [for example, L. Bréger, B. Romanowicz, L. Vinnik, *Geophys. Res. Lett*. **25**, 5 (1998)]. To test if a flat discontinuity combined with larger amplitude anomalies can produce travel time variations consistent with observations, we globally scaled the anomalies by a factor of 1.5. However, this did not significantly improve the fit to the observations.
25. Dynamic modeling incorporating a chemically distinct dense layer at the base of the mantle [for example, (*11, 14*)] demonstrates that this layer is depressed beneath cold downwellings (likely corresponding to fast seismic velocity regions) and elevated beneath hot upwellings (slow velocity regions).
26. H.-C. Nataf and S. Houard, *Geophys. Res. Lett*. **20**, 2371 (1993).
27. I. Sidorin, M. Gurnis, D. V. Helmberger, *J. Geophys. Res*. **104**, 15005 (1999).
28. For example, L. Stixrude and M. S. T. Bukowinski [*J. Geophys. Res*. **95**, 19311 (1990)] have suggested that $(Mg,Fe)SiO_3$ may break down into oxides under D″ conditions; A. M. Hofmeister (in preparation) argued that the velocity jump at the top of D″ may be due to a MgO transition to NaCl or CsCl structure.
29. A. M. Dziewonski and D. L. Anderson, *Phys. Earth Planet. Inter*. **25**, 297 (1981).
30. R. D. van der Hilst and H. Kárason, *Science* **283**, 1885 (1999).
31. It has been demonstrated (*11*) that a jump of as little as 1% in velocity may explain the observations of the shear wave D″ triplication, provided it is accompanied by sufficiently large gradients. Here, we use a slightly higher value on the premise that tomographic inversion smears the structure so that the gradients provided by the tomography models are somewhat lower than in the real structure.
32. Adding the discontinuity and the low-velocity compensation at the base of the mantle only conserves travel times of phases that do not travel through D″ or cross D″ at steep angles. The imposed low-velocity zone would disturb the travel times of phases such as *ScS*, especially at large (>80°) distances when the phase almost grazes the CMB. At shorter distances however, only a small portion of the path is affected by the basal low-velocity zone and so the travel time perturbation is less significant.
33. E. J. Garnero, D. V. Helmberger, S. Grand, *Phys. Earth Planet. Inter*. **79**, 335 (1993).
34. The seismic 1D reference models for different regions were obtained in (*7–9*) to approximate the observed differential travel times for each particular region.
35. The normalization is required for a meaningful comparison of the relative strength of *Scd* phase for paths with different epicentral distances, since *Scd*/*S* increases with distance even for a constant seismic velocity structure (*7–9*). We obtain the distance trend by averaging *Scd*/*S* amplitude ratios for all ray paths with a given epicentral distance.
36. We thank S. Grand for access to his tomography model and T. Lay and E. Garnero for providing the D″ triplication travel time data. Two anonymous reviewers provided a number of valuable comments and suggestions. Supported by NSF grant EAR-9809771. This is contribution no. 8664, Division of Geological and Planetary Sciences, California Institute of Technology.

19 July 1999; accepted 14 October 1999

Fluid Flow in Chondritic Parent Bodies: Deciphering the Compositions of Planetesimals

Edward D. Young,[1]* Richard D. Ash,[1,2] Philip England,[1] Douglas Rumble III[2]

Alteration of the Allende meteorite caused shifts in oxygen isotope ratios along a single mass fractionation line. If alteration was caused by aqueous fluid, the pattern of oxygen isotope fractionation can be explained only by flow of reactive water down a temperature gradient. Down-temperature flow of aqueous fluid within planetesimals is sufficient to explain the mineralogical and oxygen isotopic diversity among CV, CM, and CI carbonaceous chondrites and displacement of the terrestrial planets from the primordial slope 1.00 line on the oxygen three-isotope plot.

Carbonaceous chondrites comprise seven distinct groups of primitive meteorites. The groups are distinguished on the basis of mineralogy, bulk elemental concentrations, and size and proportions of constituents such as chondrules and calcium-aluminum–rich inclusions (CAIs) (*1*). Each group is characterized by distinctive oxygen isotope ratios (*2*). The diversity in mineralogy and oxygen isotopic compositions is spanned by the CV, CM, and CI groups (*3*) and has been attributed to interactions among different primordial oxygen reservoirs on distinctive parent bodies with different geological histories (*4*). Here we show that reaction between rock and flowing water inside a carbonaceous chondrite parent body could have produced zones that resemble CV, CM, and CI meteorites in mineralogy and oxygen isotope ratios.

Studies of the Allende CV3 carbonaceous chondrite using the ultraviolet laser microprobe show that increases in $^{17}O/^{16}O$ and $^{18}O/^{16}O$ at constant $\Delta^{17}O$ on an oxygen three-isotope plot (*5*) (Fig. 1) are associated with alteration. The alteration is identified by localized enrichments in Fe, Cl, and Na and by growth of secondary minerals (*6*). Alteration occurred within several million years of chondrule and CAI formation about 4.5 billion years ago (*7*) and has been attributed either to reactions between vapor and solids in the early solar nebula (*8*) or to reactions between rock and liquid water at low temperatures within parent bodies that may have resembled some present-day asteroids (*9*).

The preponderance of evidence is that water had higher $\Delta^{17}O$ values than did coexisting anhydrous silicates in the early solar system (*10*). Laser ablation analyses showing that altered and unaltered components fall on a single mass fractionation curve (Fig. 1) suggest that the $\Delta^{17}O$ of the aqueous fluid (or any other reactant) responsible for the alteration was changed from its original value to the rock value by exchange of oxygen with the rock.

The exchange of oxygen between rock and a motionless aqueous fluid cannot explain the data in Fig. 1 because, when the amount of fluid is sufficiently small that its $\Delta^{17}O$ is controlled entirely by the rock, it has too little oxygen to change rock $\delta^{17}O$ and $\delta^{18}O$. This conundrum is quantified by means of the commonly used expression for the mass balance of oxygen between reacting rock (r) and stagnant water (w)

$$\frac{N_w}{N_r} = \frac{(\delta_r - \delta_r^0)}{\delta_w^0 - (\delta_r - \Delta)} \quad (1)$$

In Eq. 1, N is the number of oxygens composing the reacting water or rock; δ is the $\delta^{18}O$ or $\delta^{17}O$ for the indicated phase after reaction; δ^0 is $\delta^{18}O$ or $\delta^{17}O$ for the indicated phase before reaction; and Δ is the difference, $\delta_r - \delta_w$, between rock and water at equilibrium. The left side of Eq. 1 is referred to as the water-rock ratio. Because Eq. 1 applies to both $\delta^{17}O$ and $\delta^{18}O$, invariant rock $\Delta^{17}O$ during the exchange of oxygen between rock and water with different initial $\Delta^{17}O$ values is only possible in the limit, where the amount of oxygen composing the water relative to the amount of oxygen composing the rock is effectively zero

$$\lim_{(N_w/N_r) \to 0} (\delta_r - \delta_r^0) = 0 \quad (2)$$

Equations 1 and 2 show that reaction between static water and rock could not have shifted rock $\delta^{18}O$ at fixed $\Delta^{17}O$ as indicated by the data in Fig. 1 unless the water and rock had

[1]Department of Earth Sciences, University of Oxford, Parks Road, Oxford, OX1 3PR, UK. [2]Geophysical Laboratory, Carnegie Institution of Washington, 5251 Broad Branch Road NW, Washington DC, 20015, USA.

*To whom correspondence should be addressed. E-mail: ed.young@earth.ox.ac.uk

identical $\Delta^{17}O$ before exchange.

Equation 1 and the restrictions it imposes on changes in rock $\delta^{18}O$ and $\Delta^{17}O$ no longer apply if the aqueous fluid flowed during isotopic exchange. Instead, mass balance during flow is satisfied by the expression

$$\alpha \mathbf{J}_{17,18_O} = -\frac{(\delta_r - \delta_r^0)}{\left(\frac{\partial \delta_w}{\partial T}\right)\nabla T} \quad (3)$$

were α is the equilibrium rock/fluid isotope ratio fractionation factor (essentially 1), $\mathbf{J}_{17,18_O}$ is a time-integrated flux of oxygen composing the fluid (as traced by ^{17}O or ^{18}O), ∇T is the gradient in temperature, and δ_r^0 represents the initial $\delta^{17}O$ or $\delta^{18}O$ for the rock at a given position. Equation 3 describes the situation where pore-filling fluid equilibrates with the host rock at each position along a fluid flow path. At every location, the fluid $\Delta^{17}O$ is controlled by the rock as long as the rock's capacity for exchange persists (*11*). Rock controls the fluid $\Delta^{17}O$ because the pore volume is generally less than the volume of the host rock, and so the bulk of the oxygen resides in the rock. Despite rock-controlled $\Delta^{17}O$, Eq. 3 shows that shifts in rock $^{17}O/^{16}O$ and $^{18}O/^{16}O$ are still possible when both $\mathbf{J}_{17,18_O}$ and ∇T are nonzero. For water flowing through rock composed primarily of silicate minerals, $(\partial \delta_w/\partial T)$ is positive and an increase in δ_r requires flow in the direction of decreasing temperature (Eq. 3); for positive $\mathbf{J}_{17,18_O}$ and $(\delta_r - \delta_r^0)$ the sign of ∇T must be negative. The increase in δ_r with alteration in Allende (Fig. 1) means that if the alteration occurred by reaction with liquid water, it did so in a hydrological system in which flow was from regions of higher temperature toward regions of lower temperature. Expressions such as Eq. 3 can lead to first-order constraints on the nature of fluid flow in a meteorite parent body, but they cannot capture the complexity that arises where fluid flux and temperature change with time along the flow path.

For this reason, we constructed finite difference models for the thermal, isotopic, and mineralogical evolution of a generic carbonaceous chondrite parent body composed of 20% water ice, 10% void space, and 70% silicate by volume (*12*). For simplicity, the silicate rock was assumed to be pure forsterite (Mg_2SiO_4). Carbon was included in the calculations because the occurrence of carbonate minerals in veins constitutes clear evidence for aqueous fluid flow, and because modeling carbonate formation allows us to compare our results with well-known differences in oxygen isotope ratios between carbonates and other minerals as a means of validation.

The components required to simulate reactions between magnesian silicate, water, and carbon can be represented by MgO, SiO_2, H_2O, and CO_2. Aqueous alteration of carbonaceous chondrites resulted in formation of phyllosilicate minerals, as evidenced most clearly by the CI and CM groups (*3*). Prevalent among these hydrous silicates is saponite, a trioctahedral smectite. In the model system, we used talc $[Mg_3Si_4O_{10}(OH)_2]$ as the $MgO\text{-}SiO_2\text{-}H_2O\text{-}CO_2$ analog for saponite and magnesite ($MgCO_3$) as the carbonate phase. Among forsterite, talc, magnesite, and a mixed aqueous fluid phase composed of H_2O and CO_2 there is one independent reaction

$$4Mg_2SiO_4 + 5CO_2 + H_2O \rightleftharpoons 5MgCO_3 + Mg_3Si_4O_{10}(OH)_2 \quad (4)$$

The progress of this reaction serves as an analog for the mineralogical effects of aqueous alteration in our calculations. The phyllosilicates in CM and CI rocks include serpentine as well as saponite (*13*). Because the fractionation of oxygen isotopes between serpentine and talc is large (*12*), we converted our model talc isotopic compositions into mixtures of 50% talc and 50% serpentine (on an oxygen basis) using published fractionation factors to compare our results with the CI and CM data.

Results reported here are for a fictive parent

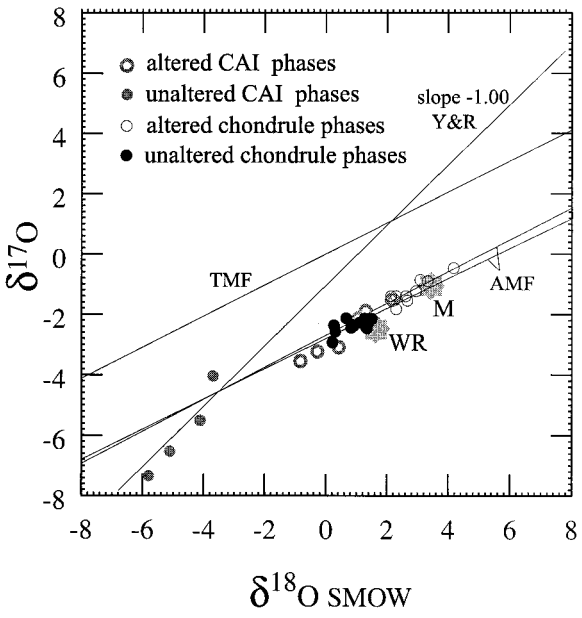

Fig. 1. Oxygen three-isotope plot showing the relative positions of the terrestrial mass fractionation curve (TMF), the slope 1.00 line (Y&R), and the Allende mass fractionation curve (AMF) defined by ultraviolet laser ablation analyses of an Allende CAI and two chondrules. The two lines for the AMF delimit physically plausible slopes between 0.51 and 0.53. Also shown are the compositions of the Allende whole rock (WR) (*22*) and bulk matrix (M) (*2*). Chondrule and CAI laser ablation analyses containing identifiable mineral grains with distinct $\Delta^{17}O$ relative to the bulk of the object are excluded for clarity.

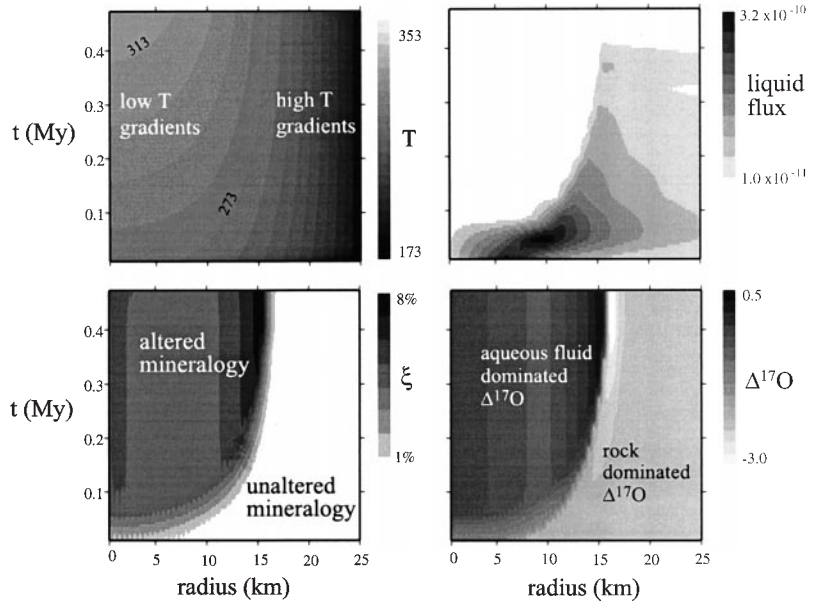

Fig. 2. Finite difference calculations portraying the temperature (in degrees kelvin), liquid flux [cubic meters of H_2O per square meter per second], mineralogical alteration (progress of Eq. 4, ξ, in mole percent), and rock $\Delta^{17}O$ evolution of a carbonaceous chondrite parent body composed of 20% by volume water ice over a period of 470,000 years. The ordinate for each plot is time in millions of years (My) after attainment of a temperature of 273 K at the core of the body.

body with a spherical radius of 25 km. Although we ignored Al in the chemical system as a way of simplifying the thermodynamic calculations, ^{26}Al was used as a heat source (*12*) with an initial $^{26}Al/^{27}Al$ consistent with formation of the body about 3 million years after formation of CAIs found in Allende (*14*). The fictive parent body was allowed to heat up from a temperature of 170 K (imposed by radiative heating from the sun) by decay of ^{26}Al. Melting of water ice above 273 K caused down-temperature flow of liquid water. Liquid was permitted to pass through rock below 273 K to simulate percolation of unfrozen water (*15*). The driving force for the down-temperature flow in a microgravity environment (g = 0.01 N/kg in this case) would likely be dominated by capillary action rather than by body forces at temperatures below the boiling point (*16*). We made no attempt to model the driving force in detail. Instead we allowed the vapor pressure of H_2O relative to the vacuum of space to drive the flow. The maximum water flux in the present model is a factor of 10 less than maximum cometary water fluxes at 1 astronomical unit (*17*). Mineralogical and isotopic reactions between the flowing liquid water and the rock were kinetically controlled (*12*).

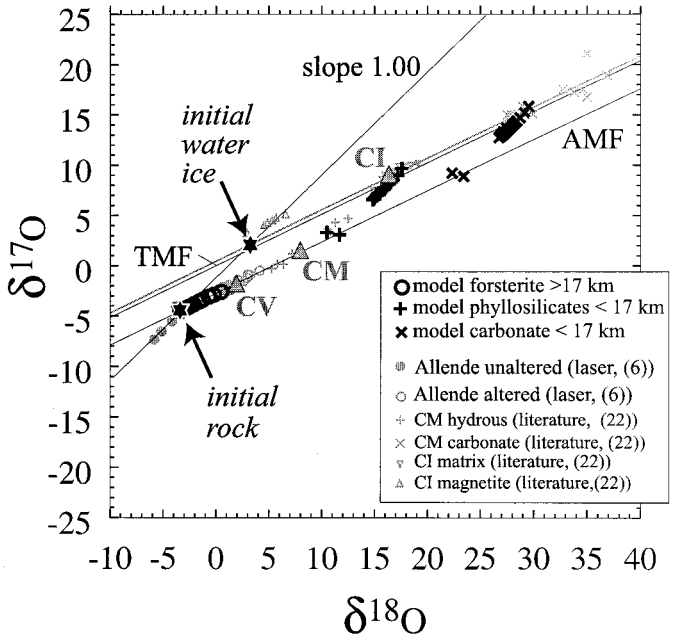

Fig. 3. Comparison between the three-isotope compositions of mineral phases from the model parent body (black symbols); whole-rock and mineral compositions from the Allende CV, Murchison CM, and Orgueil CI carbonaceous chondrite meteorites (gray symbols) (*22*); and laser ablation analyses of Allende (*6*). Meteorite whole-rock compositions are represented by the large triangles. Model phyllosilicates are mixtures of talc and serpentine from the inner 17 km of the fictive body and represent highly altered rocks. Model forsterites come from the outer 8 km of the body and make up more than 99% of the minerals by volume in this largely unaltered region. Mineral compositions were sampled at 500-m intervals from the respective zones. The fluid mass fractionation curve is shown in gray. The Allende mass fractionation curve (which is also the model rock fractionation curve), the terrestrial mass fractionation curve, and the slope 1.00 line are in black. CI magnetites are consistent with the initial water ice used in the model (right-hand black star).

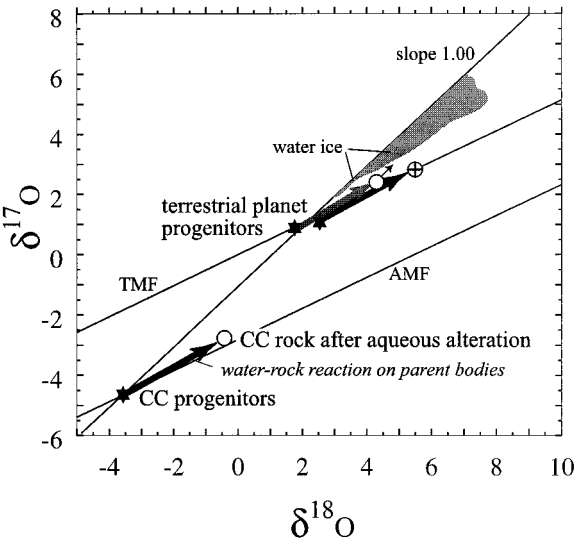

Fig. 4. Three-isotope plot showing the evolution of terrestrial (⊕), martian (♂), and carbonaceous chondrite (CC) progenitor planetesimals resulting from aqueous alteration. The magnitude of shifts in $\delta^{17}O$ and $\delta^{18}O$ resulting from the finite difference modeling presented here is shown in the lower left corner. Similar shifts place the compositions of Earth and Mars (the martian meteorites) near the slope 1.00 line. The isotopic composition of primordial water ice was apparently above the terrestrial mass fractionation curve (TMF).

We assumed that all condensed oxygen in the early solar nebula lay on the primordial slope 1.00 array on an oxygen three-isotope plot (*18*). The initial $^{17}O/^{16}O$ and $^{18}O/^{16}O$ for the rock were taken as the intersection between the slope 1.00 array and the Allende mass fractionation curve defined by laser ablation measurements of Allende. Initial $^{17}O/^{16}O$ and $^{18}O/^{16}O$ for the water ice in our calculations were defined by the intersection of the slope 1.00 array and the mass fractionation curve passing through the hydrous phases of the Orgeuil CI carbonaceous chondrite. Our choice of initial water $^{17}O/^{16}O$ and $^{18}O/^{16}O$ is consistent with magnetite oxygen isotope ratios in Orgeuil and other chondrites (*19*).

The initial CO_2 concentration of the water ice melt is constrained by forward progress of the reaction in Eq. 4. The reaction proceeds from left to right when the mole fraction of CO_2 in the fluid is greater than the equilibrium value at the appropriate conditions in the model chemical system (the equilibrium value is $<1 \times 10^{-4}$ in this case). The rate of reaction was maximized by using a CO_2 mole fraction of 0.2 in the calculations presented here. The precise starting value for CO_2 concentration is not crucial for what follows as long as it is greater than the equilibrium value.

Flow of reactive aqueous fluid through the fictive parent body produces two mineralogically distinctive zones (Fig. 2). Toward the center of the body, upstream in the radial flow system, conversion of anhydrous silicate to hydrous silicate and carbonate is extensive. Downstream toward the outer surface, there is little or no alteration. The two regions are separated by a sharp discontinuity, or front, and by a zone of maximum alteration adjacent to the front (Fig. 2). Formation of zones separated by a front and an alteration maximum were found to be salient features of the solutions regardless of the exact values for initial $^{26}Al/^{27}Al$, porosity, and ice content.

Carbonate and hydrous minerals constitute <10% molar of the rocks even in the most highly altered zone adjacent to the reaction front in Fig. 2. The values for mole percent alteration shown in Fig. 2 are averages for each model volume element. In real bodies, heterogeneous flow of fluid could have concentrated the <10% alteration into discrete, highly altered areas separated by alteration-free areas. Percentages of alteration minerals are in any case restricted by the finite supply of moving water when the volume of ice is comparable to the volume of pore space available in carbonaceous chondrites (*20*). The implication is that CI carbonaceous chondrites composed primarily of phyllosilicates, oxides, and carbonates must represent localized zones of aqueous alteration on the CI parent body (or bodies) and that such alteration was concentrated near the center of the body rather than near its surface.

The spatial pattern of isotopic alteration

mimics the mineralogical pattern (Fig. 2). Minerals upstream of the alteration front in the interior of the model body have $\Delta^{17}O$ approaching that of the original water ice, because the capacity of the rock to exchange oxygen isotopes with the fluid has been exhausted. Minerals downstream in the outer portion of the body retain the $\Delta^{17}O$ of the original rock.

The finite difference calculations confirm the first-order predictions from Eq. 3. Downstream of the alteration front in the outer part of the fictive parent body, where ∇T is negative and fluid flux is persistent (radii >17 km, Fig. 2), the range of anhydrous mineral oxygen isotope ratios caused by exchange with water is analogous to the data for Allende (Fig. 3). The small volumes of new phyllosilicate and carbonate minerals (<1% by volume) produced in the outer portion of the body have isotopic compositions that are also on the rock mass fractionation curve and have $\delta^{18}O$ values ranging up to 40 per mil (not shown in Fig. 3).

Upstream of the front within the interior of the model body (radii <17 km), hydrous silicates and carbonates are abundant in comparison to the small amounts of these minerals produced nearer to the surface. The $\delta^{17}O$ and $\delta^{18}O$ values of these new minerals approach the mass fractionation curve defined by water ice (Fig. 3). Forsterite is also driven toward the fluid $\Delta^{17}O$ in this region (not shown in Fig. 3) but does not experience the shifts toward higher $\delta^{18}O$ values along slope-1/2 lines as is the case downstream, because ∇T is small here. The pattern of oxygen isotope variability within the interior of our model parent body (radii <17 km) is similar to that defined by mineral separates from the Murchison CM and Orgueil CI carbonaceous chondrites (Fig. 3).

Figure 3 shows that the mineralogical and oxygen isotopic variability among the CV, CM, and CI groups of carbonaceous chondrites can be explained by a single process of fluid-rock reaction in parent bodies. This result is relatively insensitive to the initial isotopic value of the water ice (*21*). All that is required is one uniform oxygen reservoir for the bulk rock ($\Delta^{17}O \sim -3$ per mil) and one uniform reservoir for the aqueous fluid ($\Delta^{17}O \geq 0.5$ per mil).

Fluid-rock reactions within planetesimals may have been an important process before the final assembly of planets in the solar system. The loss of isotopically light oxygen from rock resulting from exchange with escaping water would have led to an increase in planetesimal $\delta^{17}O$ and $\delta^{18}O$ values (Fig. 4). In the model presented here, 25% of the water ice is lost from the body. The increase in rock $\delta^{18}O$ is about 3 per mil, and the attendant increase in $\delta^{17}O$ results in a slight increase in $\Delta^{17}O$ of several tenths per mil. Subtraction of comparable effects from the bulk oxygen isotopic compositions of Earth and Mars (the martian meteorites) places the oxygen composition of progenitor planetesimals for the terrestrial planets on or near the slope 1.00 array (Fig. 4), removing the necessity for distinct primordial oxygen reservoirs other than the slope 1.00 array.

References and Notes

1. A. J. Brearley and R. H. Jones, *Rev. Mineral.* **36**, 3 (1999).
2. R. N. Clayton and T. K. Mayeda, *Geochim. Cosmochim. Acta* **63**, 2089 (1999).
3. CV, CM, and CI refer to carbonaceous chondrites (C) with chemical similarities to the Vigarano (V), Mighei (M), and Ivuna (I) meteorites, respectively [J. T. Wasson, *Meteorites: Their Record of Early Solar System History* (Freeman, New York, 1985)]. CIs and CMs tend to be richer in volatile elements (such as S, Fe, K, and Na) than CVs. CIs are composed of hydrous minerals and have fractures filled with carbonate and sulfate minerals, whereas CVs are composed primarily of anhydrous minerals. CMs are intermediate, with roughly half of the minerals by weight being anhydrous.
4. A. Meibom and B. E. Clark, *Meteorit. Planet. Sci.* **34**, 7 (1999).
5. On a three-isotope plot, $\delta^{17}O$ (ordinate) is plotted against $\delta^{18}O$ (abscissa). $\delta^{17}O$ refers to the per mil deviation in a sample $^{17}O/^{16}O$ from a standard, in this case standard mean ocean water (SMOW), expressed as $\delta^{17}O = [(^{17}O/^{16}O)_{sample}/(^{17}O/^{16}O)_{SMOW} - 1]\ 1000$. Values of $\delta^{18}O$ are defined in an analogous fashion. Mass fractionation curves with slopes between 0.51 and 0.53 define changes in oxygen isotope ratios that result from physicochemical processes, including evaporation, diffusion, and most chemical reactions. The terrestrial mass fractionation curve characterizes Earth's homogeneous oxygen reservoir [F. Robert, A. Rejou-Michel, M. Javoy, *Earth Planet. Sci. Lett.* **108**, 1 (1992)]. $\Delta^{17}O$ refers to deviations in $\delta^{17}O$ from the terrestrial mass fractionation curve at the corresponding value for $\delta^{18}O$ ($\Delta^{17}O \simeq \delta^{17}O - 0.52\ \delta^{18}O$). $\Delta^{17}O$ is a measure of the intercept for a mass fractionation curve and can be used to define the position of the curve on a three-isotope plot.
6. R. D. Ash, E. D. Young, D. Rumble III, G. J. MacPherson, *Lunar Planet. Sci. Conf.* **XXX**, CD-ROM (1999); E. D. Young and S. S. Russell, *Science* **282**, 452 (1998).
7. T. D. Swindle, M. W. Caffee, C. M. Hohenberg, *Geochim. Cosmochim. Acta* **52**, 2215 (1988); C. J. Allègre, G. Manhès, C. Göpel, *Geochim. Cosmochim. Acta* **59**, 1445 (1995); A. N. Krot *et al.*, *Meteorit. Planet. Sci.* **34**, 67 (1999).
8. A. Hashimoto, *Geochim. Cosmochim. Acta* **56**, 511 (1992).
9. A. N. Krot, E. R. D. Scott, M. E. Zolensky, *Meteoritics* **30**, 748 (1995).
10. Step heating of CM carbonaceous chondrite hydrous phases in the laboratory liberates water with $\Delta^{17}O$ greater than the bulk silicate $\Delta^{17}O$ [T. K. Mayeda and R. N. Clayton, *Lunar Planet. Sci. Conf.* **XXIX**, CD-ROM (1998); L. Baker, I. A. Franchi, J. M. Maynard, I. P. Wright, C. T. Pillinger, *Lunar Planet. Sci. Conf.* **XXIX**, CD-ROM (1998)]. Magnetites from ordinary and carbonaceous chondrites are thought to be composed of oxygen derived from an oxidizing aqueous fluid [A. J. Brearley and R. H. Jones, *Rev. Mineral.* **36**, 3 (1999)], and their higher $\Delta^{17}O$ as compared with that of anhydrous silicate minerals suggests higher $\Delta^{17}O$ for water relative to anhydrous rock [M. W. Rowe, R. N. Clayton, T. K. Mayeda, *Geochim. Cosmochim. Acta* **58**, 5341 (1994); B. Choi, K. D. McKeegan, A. N. Krot, J. T. Wasson, *Nature* **392**, 577 (1998)].
11. Equation 3 applies where the oxygen isotope exchange capacity of the rock has not been exhausted by protracted equilibration with flowing fluid [E. D. Young, in *Reviews of Geophysics Supplement U.S. National Report to International Union of Geodesy and Geophysics 1991–1994* (American Geophysical Union, Washington, DC, 1995), p. 41]. Analytical equations that describe the effects of rock exchange capacity depletion are given by G. M. Dipple and J. M. Ferry [*Geochim. Cosmochim. Acta* **56**, 3539 (1992)].
12. The parent body was modeled as a sphere with the use of explicit finite difference. Temperatures at each time step were obtained by solving the energy conservation equation $(\partial T/\partial t) = \kappa(\partial^2 T/\partial r^2 + 2/r\ \partial T/\partial r) + (1 - \phi)Q/C$, where t is time, T is temperature, κ is thermal diffusivity, r is radial distance, Q is heat production, ϕ is porosity + ice fraction, and C is specific heat. Constants not specified derive from the literature [R. E. Grimm and H. Y. McSween Jr., *Icarus* **1989**, 244 (1989)]. The value for Q was prescribed by 4.003×10^6 eV per ^{26}Al decay (decay constant $\lambda = 9.76 \times 10^{-7}$ year^{-1}); an Al mass concentration of 13.05×10^{-3} [J. T. Wasson and G. W. Kallemeyn, *Philos. Trans. R. Soc. London Ser. A* **325**, 535 (1988)]; and an initial $^{26}Al/^{27}Al^{o}$, yielding $Q = 6 \times 10^{-3}$ $(^{26}Al/^{27}Al)^{o}$ $\exp(-\lambda t)$ in watts per kilogram. The latent heats of ice melting and mineral-fluid reaction tend to cancel and do not affect the salient features of the model [L. Wilson, K. Keil, L. B. Browning, A. N. Krot, *Lunar Planet. Sci. Conf.* **XXIX**, CD-ROM (1998)]. Isotope ratios were obtained by solving the conservation equation $(\partial C_f/\partial t) = -\nabla(C_f\vec{v}) + R_{rxn} + R_{melt}$, where C_f is the concentration of ^{17}O or ^{18}O in the fluid (moles per volume), $\vec{v}$ is fluid pore velocity, R_{rxn} is the rate of ^{18}O or ^{17}O production by reaction with minerals, and R_{melt} is the rate of production due to melting ice. We used the kinetic expression $R_{rxn} = L[(\beta/\alpha)C_s - C_f]$ for the rate of ^{17}O or ^{18}O production by fluid-rock exchange, where C_s is the concentration in the solid, L is the phenomenological rate constant (1×10^{-9} s^{-1} for the model presented here), β is the ratio of moles of O per volume fluid to moles of O per volume bulk solid, and α is the solid-fluid isotope fractionation factor. For the rate of isotopic production due to ice melting, we used $R_{melt} = C_{ice}k\ (RT)/(P_{eq}\hat{V})$, where R is the ideal gas constant, P_{eq} is the equilibrium vapor pressure of H_2O, $\hat{V}$ is the molar volume of water vapor, and k is a rate constant reflecting the thermal properties of ice (10^{-15} s^{-1} in the present calculations). Isotopic concentrations for individual minerals were obtained from the bulk by satisfying equilibrium mass fractionation and mass balance among the solid phases. Fractionation factors were taken from the literature [Y. Zheng, *Earth Planet. Sci. Lett.* **120**, 247 (1993); D. A. Northrop and R. N. Clayton, *J. Geol.* **74**, 174 (1966); R. N. Clayton and S. W. Kieffer, *Stable Isotope Geochemistry: A Tribute to Samuel Epstein* [Geochemical Society Special Publication **3**, 3 (1991)]; Y. Matsuhisa, J. R. Goldsmith, R. N. Clayton, *Geochim. Cosmochim. Acta* **42**, 1131 (1979)]. For the reaction progress of Eq. 4, ξ, at each position and time we used $(d\xi/dt) = L'A$ where L' is the phenomenological rate constant and A is the reaction affinity. We used $L' = 2.0/(RT)\ \exp[-6.3 \times 10^4/(RT)]$ in mol^2/(J m^3 s) [G. W. Fisher, *Geochim. Cosmochim. Acta* **42**, 1035 (1978)] and $A = -\Delta\mu^{T,*,o} + RT \ln f_{H_2O} + 5\ RT \ln f_{CO_2}$, where $\Delta\mu^{T,*,o}$ is the change in molar Gibbs free energy for the standard state pure species at 1 bar and T due to reaction (derived from standard tables) and f_i are fugacities. The fugacity coefficient for H_2O was 0.18, whereas that for CO_2 was calculated using $\gamma_{CO_2} = 1.0/[7.0 \times 10^{-9} \exp(0.0279T)]$, representing a parameterization of the equilibrium concentrations of CO_2 in coexisting aqueous liquid and vapor [A. J. Ellis, *Am. J. Sci.* **257**, 217 (1959)]. Concentrations of CO_2 (for $\ln f_{CO_2}$) were calculated from the conservation equation for CO_2 in the fluid phase: $(\partial C_f^{CO_2}/\partial t) = -\nabla(C_f^{CO_2}\vec{v}) - (5/\phi)\ L'\ A + C_{ice}^{CO_2}\ k(RT)/(P_{eq}\hat{V})$, where $C_f^{CO_2}$ and $C_{ice}^{CO_2}$ are the concentrations (molarities) of CO_2 in fluid and water ice, respectively. CO_2 in ice is either original to the condensed water ice or reflects rapid oxidation of carbon upon melting. The rate of ice melting, $R_{s\rightarrow l} = k(RT)/(P_{eq}\hat{V})$, determined the liquid velocity $\vec{v}$ within each representative elementary volume i according to the relation $\vec{v}_i = \Sigma_{j<i}R_{s\rightarrow l,j}V_{rev,j}/(4\pi r_i^2)$ where $V_{rev,j}$ is the volume of spherical shell j.
13. A. E. Rubin, *Meteorit. Planet. Sci.* **32**, 321 (1997).
14. The initial $^{26}Al/^{27}Al$ ratio was 1.7×10^{-6} and represents about 3 million years of decay from a canonical $^{26}Al/^{27}Al$ ratio of 5×10^{-5}. The latter is thought to characterize CAIs in carbonaceous chondrites [A. K. Kennedy, J. R. Beckett, D. A. Edwards, I. D. Hutcheon, *Geochim. Cosmochim. Acta* **61**, 1541 (1997)].
15. Interfacial liquid water at subfreezing temperatures, referred to as unfrozen water, is known to migrate through frozen terrestrial soils [M. S. Seyfried and M. D. Murdock, *J. Hydrol.* **202**, 95 (1997)]. J. M. Rietmeijer

[*Nature* **313**, 293 (1985)] postulated that hydrous silicates could have been produced by reaction with unfrozen water on carbonaceous chondrite parent bodies. Calorimetric experiments demonstrate that carbonaceous chondrites can host unfrozen water [J. L. Gooding, *Lunar Planet. Sci. Conf.* **XV**, 228 (1984)].

16. S. B. Jones and D. Or, *Water Res. Res.* **35**, 929 (1999); Y. Taitel and L. Witte, *Chem. Eng. Sci.* **51**, 695 (1996).
17. D. W. G. Sears, H. W. Kochan, W. F. Huebner, *Meteorit. Planet. Sci.* **34**, 497 (1999).
18. E. D. Young and S. S. Russell, *Science* **282**, 452 (1998); S. S. Russell, L. A. Leshin, K. D. McKeegan, G. J. Macpherson, *Meteorit. Planet. Sci.* **32**, A88 (1997); S. Sahijpal, K. D. McKeegan, A. N. Krot, D. Weber, A. A. Ulyanov, *Meteorit. Planet. Sci.*, **34**, A101 (1999).
19. Magnetites precipitated from oxidation of Fe in an aqueous environment should have $\delta^{18}O$ values near that of water or several per mil lower than water on a mass fractionation curve. Equilibrium oxygen isotope fractionation between magnetite and liquid H_2O ($\delta^{18}O$ magnetite $-$ $\delta^{18}O$ H_2O) at 273 K is -0.1 per mil [Y. Zheng, *Geochim. Cosmochim. Acta* **55**, 2299 (1991)]. At the maximum temperatures that apply in our model ($\leq$323 K) the equilibrium $\delta^{18}O$ value for magnetite is 5 per mil lower than the $\delta^{18}O$ of coexisting H_2O. Magnetites from various chondrite groups lie on or near the slope 1.00 array or several per mil to the left of the array (lower $\delta^{18}O$) [B. Choi, K. D. McKeegan, A. N. Krot, J. T. Wasson, *Nature* **392**, 577 (1998); M. W. Rowe, R. N. Clayton, T. K. Mayeda, *Geochim. Cosmochim. Acta* **58**, 5341 (1994)], which is consistent with what is expected, based on the initial equilibrium partitioning between magnetite and water on the slope 1.00 line.
20. Bulk porosities of carbonaceous chondrite groups range from 10 to 30% by volume [L. Wilson, K. Keil, S. J. Love, *Meteorit. Planet. Sci.* **34**, 479 (1999)].
21. The initial $\delta^{17}O$ and $\delta^{18}O$ values for the water ice used in the model presented in this report are 2 and 3 per mil, respectively. Using initial values of 20 and 30 per mil for the water, as suggested by R. N. Clayton and T. K. Mayeda [*Earth Planet. Sci. Lett.* **67**, 151 (1984)], results in no appreciable change in our results downstream of the front, whereas the isotopic compositions of the phyllosilicate and carbonate minerals upstream of the front are similar to those in Fig. 3 but are displaced by approximately $+4$ per mil in $\delta^{18}O$ and $+3$ per mil in $\delta^{17}O$, resulting in a somewhat poorer fit to the CM and CI data.
22. Conventional fluorination data are from R. N. Clayton and T. K. Mayeda [*Earth Planet. Sci. Lett.* **67**, 151 (1984)] and from M. W. Rowe, R. N. Clayton, and T. K. Mayeda [*Geochim. Cosmochim. Acta* **58**, 5341 (1994)]. Secondary ion mass spectrometry analyses of Murchison CM carbonate were reported by A. J. Brearley, J. M. Saxton, I. C. Lyon, and G. Turner [*Lunar Planet. Sci. Conf.* **XXX**, CD-ROM (1999)].
23. Supported by a grant from the Particle Physics and Astronomy Research Council (PPA/G/S/1998/00069) of the United Kingdom.

3 August 1999; accepted 14 October 1999

Imaging of Humic Substance Macromolecular Structures in Water and Soils

S. C. B. Myneni,[1,3]* J. T. Brown,[2] G. A. Martinez,[4] W. Meyer-Ilse[2]

Humic substances (HSs) are the natural organic polyelectrolytes formed from the biochemical weathering of plant and animal remains. Their macromolecular structure and chemistry determine their role in biogeochemical processes. In situ spectromicroscopic evidence showed that the HS macromolecular structures (size and shape) vary as a function of HS origin (soil versus fluvial), solution chemistry, and the associated mineralogy. The HSs do not simply form coils in acidic or strong electrolyte solutions and elongated structures in dilute alkaline solutions. The macromolecular structural changes of HSs are likely to modify contaminant solubility, biotransformation, and the carbon cycle in soils and sediments.

Aqueous humic substances (HSs) exist primarily as soluble ions at low concentration and form colloids and precipitates at high concentration and when they react with cations and protons (*1, 2*). These changes can alter the HS macromolecular structures and subsequently affect the chemistry of HS coatings on mineral and colloid surfaces, the stability of organomineral aggregates, and the retention of pollutants and C in soils and sediments (*3–5*). Hence, direct information on the magnitude of changes in HS macromolecular structures, as a function of solution and substrate mineral chemistry, and their origin is critical for understanding the geochemical reactions mediated by natural organic molecules (*6*).

To test the influence of these parameters on natural organic molecule configuration, we conducted experiments on humic and fulvic acids isolated from river water (Suwannee River, Georgia), peat (Belle Glade, Florida), and soil (Mollic Epipedon, Illinois) samples. Fulvic and humic acid samples were the HS fractions isolated at alkaline and acidic pH, respectively, by the International Humic Substance Society and have been previously characterized (*7, 8*). The solution compositions tested were pH (2 to 12, adjusted with HCl or NaOH), ionic strength (0.01 to 2 M NaCl or 0.01 to 2 M $CaCl_2$), HS concentration (0.03 to 10 g of C liter^{-1}), and counterion composition (1 mM Cu^{2+} or Fe^{3+}). The influence of substrate mineralogy was examined for goethite (α-FeOOH), calcite ($CaCO_3$), and clays (kaolinite and montmorillonite), which are common to several soils and sediments (*9*). To correlate the macromolecular structures of isolated HSs with those of undisturbed natural samples, we also examined soil organic molecules in their pristine stage (organic molecules not extracted from surrounding soil matrix) for an Ultisol (Aquic Tropohumult, Puerto Rico) and an Alfisol (Kesterson Reservoir, California). These soils formed under contrasting chemical conditions with pH values of 5 and 8.0, respectively, and an organic C concentration of 1.5 and 0.3%, respectively. The macromolecular structures of HSs under these chemical conditions were examined directly at the high-resolution spectromicroscopy facility at the Advanced Light Source [Lawrence Berkeley National Laboratory (LBNL)] (*10*). The sample images were collected at the following x-ray photon energies: in the water window (516.6 eV) and at the Fe L (697 and 706 eV) and Cu L (933 and 936 eV) absorption edges. The contrast in images collected at the water window is dominated by the mass absorption of C and N atoms in the sample and helps in the determination of HS macromolecular structures. The images at the Fe and Cu edges, together with those obtained at the water window, are useful for examining cation and mineral association with HSs.

We examined the Suwannee River fulvic acid isolates with an x-ray microscope and found that they did not exhibit any measurable structures below a HS concentration of 1.0 g of C liter^{-1}. As the concentration was increased above 1.3 g of C liter^{-1}, HSs formed aggregates of different shapes and sizes (Fig. 1). In dilute, acidic, high-ionic-strength NaCl solutions, HSs predominantly formed globular aggregates and ringlike structures (Fig. 1A). As the fulvic acid concentration was increased, large sheetlike structures also formed and enclosed these smaller structures. Visible coiling was uncommon, and the HSs dispersed completely into aggregates of small size ($<$0.1 μm) in solutions of pH $>$ 8.0 (Fig. 1B). Although the addition of 1 M NaCl did not favor coiling under these alkaline conditions, concentrated HS solutions formed globular aggregates bound together with thin films of HSs. Additions of di- and trivalent cations to HS solutions promoted their precipitation at low C concentration and displayed macromolecular structures different from those formed in the presence of monovalent ions. In dilute fulvic acid solutions of Ca^{2+}, Cu^{2+}, or Fe^{3+}, the fulvic acids formed thin thread- and netlike structures (Fig. 1, C and D). As the fulvic acid and cation concentrations increased, these structures grew larger and formed rings and sheets (see Web fig. 1, available at www.sciencemag.org/feature/data/1043547.shl).

[1]Earth Sciences Division, [2]Center for X-ray Optics, Lawrence Berkeley National Laboratory, Berkeley, CA 94720, USA. [3]Department of Geosciences, Princeton University, Princeton, NJ 08544, USA. [4]Agriculture Experimental Station, University of Puerto Rico, Rio Piedras, PR 00928, USA.

*To whom correspondence should be addressed. E-mail: smyneni@princeton.edu